Active matter commensuration and frustration effects on periodic substrates

C. Reichhardt and C. J. O. Reichhardt

Theoretical Division and Center for Nonlinear Studies, Los Alamos National Laboratory, Los Alamos, New Mexico 87545, USA

(Received 4 November 2020; accepted 13 January 2021; published 3 February 2021)

We show that self-driven particles coupled to a periodic obstacle array exhibit active matter commensuration effects that are absent in the Brownian limit. As the obstacle size is varied for sufficiently large activity, a series of commensuration effects appear in which the motility induced phase separation produces commensurate crystalline states, while for other obstacle sizes we find frustrated or amorphous states. The commensuration effects are associated with peaks in the amount of sixfold ordering and the maximum cluster size. When a drift force is added to the system, the mobility contains peaks and dips similar to those found in transport studies for commensuration effects in superconducting vortices and colloidal particles.

DOI: 10.1103/PhysRevE.103.022602

I. INTRODUCTION

Commensuration effects arise in a variety of hard and soft matter systems when an assembly of particles is coupled to a periodic substrate with a spacing that matches the average interparticle spacing. Such effects occur for the ordering of atoms or molecules on surfaces [1–3], vortices in superconductors or Bose-Einstein condensates with periodic pinning arrays [4–7], colloidal particles on optical trap arrays [8–10] or patterned surfaces [11], and cold atoms on optical lattices [12]. Conversely, if the particle assembly cannot fit within the constraints imposed by the substrate, then frustration can cause the disordering of the system or the formation of localized defects such as kinks or antikinks [13,14]. Commensuration effects also strongly modify the transport properties under an applied drive in these systems, producing reduced transport or enhanced pinning when a commensuration occurs and generating a series of peaks or dips in the transport coefficients as the parameters are varied [5,6,13–17].

Coupling of active matter or self-driven particles to a substrate [18,19] has been realized in numerous experiments [18–22]. Many active particles have only short range repulsive interactions, so the system forms a uniform liquid at lower densities in the nonactive or Brownian limit; however, when activity is present, the particles undergo a self-clustering or motility induced phase separation into a high density crystalline phase surrounded by a low density gas [20,21,23–25]. Although there have been various methods proposed for coupling an active matter system to random [19,22,26–32] or periodic obstacle arrays [33–38], the possible commensuration effects that could occur on a periodic substrate in active systems have not been considered before now, to our knowledge. For a two-dimensional (2D) system of disks in the Brownian or zero activity regime, commensuration effects do not arise until the disk density ϕ is high enough for all of the disks to touch each other, so, for a nonactive system at $\phi < 0.8$, commensuration effects should be absent. In such high density nonactive systems, a series of commensuration effects appear when the number of disks is an integer multiple of the number of obstacles or pinning sites [15]. Since thermal effects typically wash out commensuration effects [15], it might be expected that active matter systems would not exhibit any commensuration effects.

Here we examine a 2D active matter system of self-propelled run-and-tumble disks interacting with a square array of obstacles. For certain obstacle sizes, we find that the system can undergo a strong motility-induced phase transition into a crystalline state that is commensurate with the obstacle lattice and that coexists with a low density gas. For other obstacle sizes, the motility-induced phase separation produces an amorphous crystal due to a frustration effect caused by a mismatch between the active disk spacing and the obstacle spacing. The spacing of the disks in the motility-induced dense phase is key in determining whether commensurate or incommensurate behavior occurs. The commensuration effects produce peaks in the size of the largest cluster and in the amount of sixfold ordering. A variety of different commensurate states appear, including states with local square ordering, aligned states, and sliding crystalline states. Under an applied drift force, the transport is a strongly nonmonotonic function of the obstacle size and exhibits dips at commensurate states as well as peaks at incommensurate or frustrated states. For the range of densities we examine, the commensuration effects are absent in the Brownian limit and become stronger for increasing activity or longer run times.

II. SIMULATION AND SYSTEM

We model a 2D system of N_a active run-and-tumble disks of density ϕ_a interacting with a periodic array of $N_{\rm obs}$ obstacles composed of posts of diameter d and lattice constant a. The overdamped equation of motion for an active disk i is given by

$$\alpha_d \mathbf{v}_i = \mathbf{F}_i^{dd} + \mathbf{F}_i^{m} + \mathbf{F}_i^{obs} + \mathbf{F}_i^{D}, \tag{1}$$

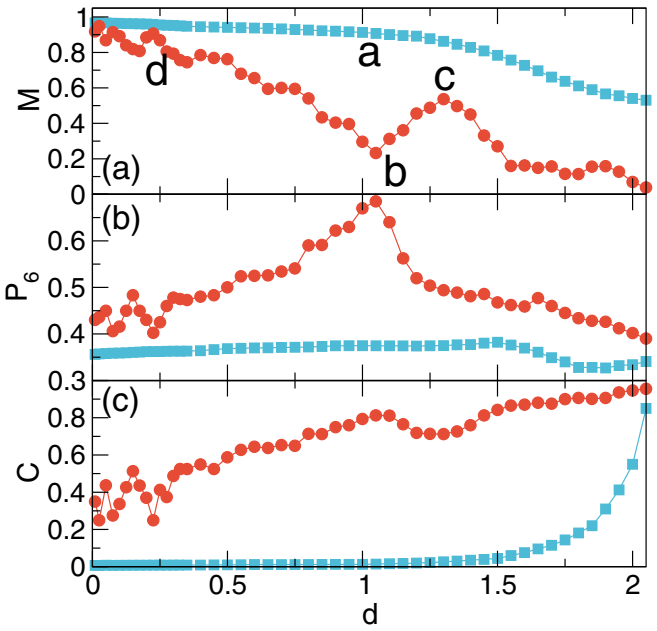

FIG. 1. Behavior of an active disk system with $d_a = 0.9$ for a run length of $l_r = 0.025$ (squares) in the Brownian limit and $l_r = 175$ (circles) in the active limit. (a) Mobility M vs obstacle diameter d. (b) Fraction of sixfold coordinated particles P_6 vs d. (c) Size of the largest cluster C vs d. The letters a–d in panel (a) indicate the points corresponding to the images in Fig. 2.

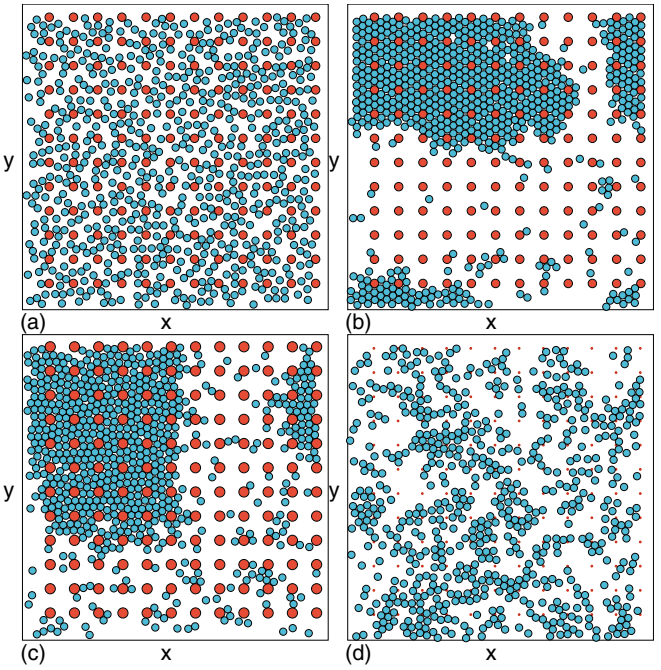

FIG. 2. Snapshots of the active disk positions (blue circles) and the obstacles (red circles) for the system in Fig. 1 with $d_a = 0.9$. (a) A uniform liquid at $d = 1.05$ and $l_r = 0.025$. (b) At $d = 1.05$ and $l_r = 175$, there is a phase separated state in which the dense regions form a commensurate solid. (c) At $d = 1.3$ and $l_r = 175$, there is a phase separated amorphous or frustrated state. (d) A frustrated state at $d = 0.225$ and $l_r = 175$. Movies illustrating the commensurate and incommensurate states can be found in the Supplemental Material [39].

where the damping constant $\alpha_d = 1.0$, and $\mathbf{r}_i$ and $\mathbf{v}_i = d\mathbf{r}_i/dt$ are the position and velocity of disk i. For the disk-disk interaction force $\mathbf{F}_i^{dd}$, we use a harmonic repulsion with spring constant k_a and disk radius r_a, so that the disk diameter is $d_a = 2r_a$. We set $k_a = 150$, which is large enough to keep the disk-disk overlap in our study below one percent. The disk-obstacle force $\mathbf{F}^{obs}$ is also modeled as a harmonic potential. The active disk coverage is $\phi_a = N_a \pi r_a^2/L^2$, where the system size is $L \times L$ with $L = 36$, and the combined coverage of the disks and obstacles is $\phi_{\rm tot}$. For the self-propulsion of the active disks $\mathbf{F}^m$, a force F_m is applied in a randomly chosen direction for a run time of τ_r, after which the motor force instantaneously reorients to a new randomly chosen direction for the next run time. The motor force is held fixed to the value $F_m = 1.0$, and all particles in the system have the same value of τ_r. We characterize the system by the run length $l_r = F_m \tau_r$, the distance an isolated active particle would move during the run time τ_r. Run times are reported in terms of simulation time steps, each of which is equivalent to 0.002 units of dimensionless time. We also consider the effects of an external drive $\mathbf{F}^D = F_D \hat{\mathbf{x}}$ and measure the mobility M using the average velocity in the driving direction, $\langle V_x \rangle = \sum_{i=1}^{N^d} \mathbf{v}_i \cdot \mathbf{x}$. We define $M = \langle V_x \rangle / V_{\rm free}$, where $V_{\rm free}$ is the average velocity that would appear under the same driving force in the absence of any obstacles. Unless otherwise noted, we fix $a = 3.0$ and $F_D = 0.2$, and vary d_a, d, and l_r.

III. RESULTS

In Figs. 1(a)–1(c) we plot the mobility M, the fraction of sixfold coordinated particles P_6, and the fraction of particles in the largest cluster C versus the obstacle diameter d for a system with $\phi_a = 0.32$, $N_a = 656$, $N_{\rm obs} = 144$, and $d_a = 0.9$ averaged over 100 realizations. We show two run length values: $l_r = 0.025$, where the system is in the Brownian limit, and $l_r = 175$, the active limit where an obstacle free system would exhibit motility induced phase separation. For the short run length of $l_r = 0.025$, M has an initial value near 1.0 and exhibits a monotonic decrease with increasing d, while P_6 is mostly flat and C starts to increase due to the onset of drive-induced clogging once $d > 1.5$. For the active limit of $l_r = 175$, M also has an initial value near 1.0 but changes nonmonotonically with increasing d, showing a pronounced dip near $d = 1.05$ which correlates with a peak in P_6 and a smaller peak in C. There is also a peak in M near $d = 1.3$ that is associated with a drop in P_6 and a smaller dip in C. Additional features include a peak in M near $d = 0.2$ and a smaller peak near $d = 1.75$.

In Fig. 2(a) we show a snapshot of the active particles and the obstacles for the system in Fig. 1 at $l_r = 0.025$ and $d = 1.05$, where a uniform liquid state appears. By comparison, in Fig. 2(b) a sample with $l_r = 175$ at $d = 1.05$ forms a phase separated state of high density coexisting with a low density gas. This combination of parameters corresponds to the peak in P_6 and the dip in M in Fig. 1. In Fig. 3(a) we show a blowup of the high density region from Fig. 2(b), indicating more clearly that the system forms a triangular lattice which is commensurate with the underlying square array. Figure 2(c)

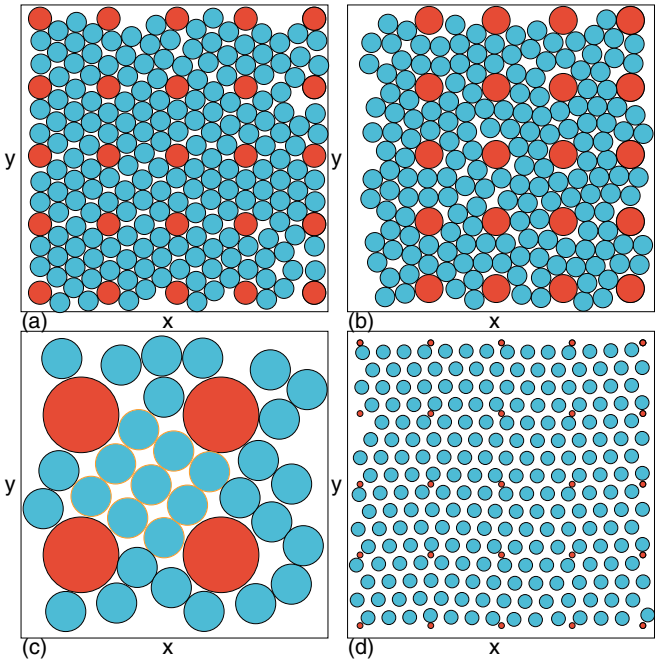

FIG. 3. Snapshots of the active disk positions (blue circles) and the obstacles (red circles) for the system in Fig. 1 with $d_a = 0.9$. (a) A blowup of the dense region in Fig. 2(b) at $d = 1.05$ and $l_r = 175$, showing triangular commensurate ordering. (b) A blowup of the dense region in Fig. 2(c) at $d = 1.3$ and $l_r = 175$, which is in an amorphous state. (c) A blowup illustrating the local square ordering at $d = 1.7$ and $l_r = 175$. (d) A larger subsection of the system for $d = 0.15$ and $l_r = 175$ showing a sliding crystal phase. For clarity, the size of the mobile disks has been reduced in panel (d).

illustrates the system in Fig. 1 at $l_r = 175$ and $d = 1.3$, corresponding to a local maximum in M and a drop in P_6. Although the system still shows clustering, the structure of the active disks in the dense region is now amorphous, as shown more clearly in Fig. 3(b). The disorder is produced by a frustration effect that arises when the natural spacing of the active crystal does not match the spacing of the interstitial region between the obstacles. The peak in M is similar to the increase in motion or decrease in the critical depinning force found in nonactive commensurate systems at incommensurate densities [5,6,13–15]. In the nonactive systems, the commensurate crystalline states have a higher shear modulus and can be more strongly pinned by the obstacles. In contrast, for the frustrated system the shear modulus is reduced, permitting the particles to move more easily and producing minima in the depinning force of the incommensurate state. Near $d = 0.2$ for the active system in Fig. 1, a peak in M and a dip in P_6 appear at another incommensurate region where the disks are disordered, as shown in Fig. 2(d) for $d = 0.225$. For sufficiently large d in Fig. 1(c), the cluster size C rises with increasing d even in the Brownian limit. This is the result of the piling up of disks behind the obstacles into clogged states. Such clogging for a nonactive system of disks driven through an obstacle array was studied elsewhere [40]. Figure 1(c) illustrates that the clustering effects are significantly enhanced in the active system for all values of d.

The strong peak in P_6 for the active system in Fig. 1(b) indicates that a large fraction of the disks have sixfold ordering; however, this does not necessarily mean that long range order is present, since phase separated clusters can form which contain uncorrelated patches of sixfold order. Additionally, even within a particular dense region there can be multiple orientations of the sixfold ordering. This is similar to what occurs in many commensurate systems, which often contain grain boundaries separating different degenerate configurations [15]. The sixfold ordering is clearly enhanced for obstacle sizes d at which the commensuration effects and associated reduction in mobility appear. Other characterization methods such as an orientational order parameter can be used, but since the disk density is strongly nonuniform in the clustered state, this type of measurement shows strong fluctuations. Even for the measures we consider in Fig. 1, the fluctuations become strong for small $d < 0.25$. This occurs due to the formation of partially clustered phases that break apart rapidly; however, the peak in M and minima in P_6 and C at $d = 0.25$ are robust features that persist as we vary the initial conditions. The strong fluctuations at small d can also result when the number of degenerate commensurate structures becomes very large. The two prominent features at points b and c in Fig. 1 are extremely robust and would be ideal for experimental observation.

For $d > 1.5$, a distinctive type of active cluster appears which has local square short-range ordering within a single plaquette. These clusters are associated with a drop in M and an increase in C. An example of the $d = 1.7$ clustered state appears in Fig. 3(c), where a single plaquette with local square ordering is highlighted. As d increases further, other types of commensurate crystals can occur.

In the active system near $d = 0.15$, where there is a smaller peak in C, the disks form a sliding crystalline state in which the commensuration effect is determined by the number of rows of active disks that can fit between adjacent rows of obstacles, as shown in Fig. 3(d) where we highlight a subsection of the system containing four rows of disks. The sliding crystal exhibits intermittent jumping between crystal and disordered states, causing the value of P_6 to be reduced compared to the commensurate state which appears at higher d. If we consider a random array of obstacles, we do not observe any commensurate effects but instead find a monotonic decrease of the mobility with increasing d.

In Fig. 4(a) we plot M versus d for the system in Fig. 1 with fixed $d_a = 0.9$ at varied $l_r = 0.00025$, 0.01, 0.025, 0.25, 40, 175, and 1750. The overall mobility decreases with increasing l_r, while commensuration effects only appear once $l_r > 10$, which coincides with the running length at which self-clustering begins to occur. The commensuration effects become sharper as l_r increases. For large d and large l_r, the mobility drops to zero when the system enters an active jammed or clogged state, while for smaller l_r at high d, the flow is reduced but remains finite.

Figure 4(b) shows M versus d for the system in Fig. 1 with fixed $l_r = 175$ and varied active disk diameter of $d_a = 0.7$, 0.8, 0.9, and 1.0, giving $\phi_a = 0.195$, 0.254, 0.32, and 0.4, respectively. For $d_a = 0.7$, no clustering occurs until $d > 1.5$, which correlates with a drop in M when a commensurate state forms with a structure that is similar to that illustrated in

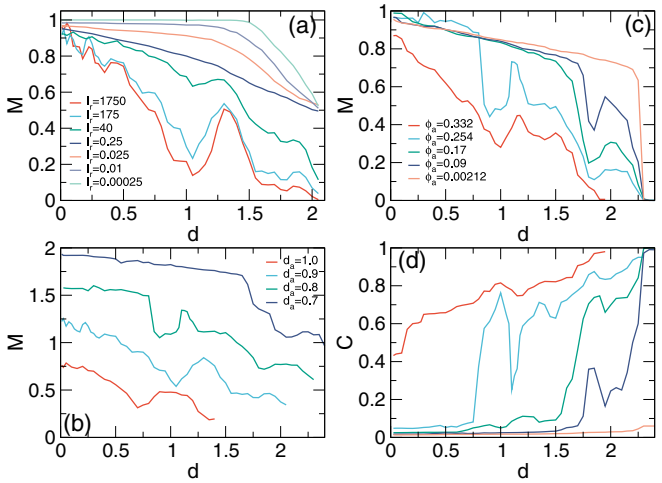

FIG. 4. (a) M vs d for the system in Fig. 1 for $l_r = 0.00025$, 0.01, 0.025, 0.25, 40, 175, and 1750, from top to bottom. (b) M vs d for $l_r = 175$ at $d_a = 0.7$, 0.8, 0.9, and 1.0, from top to bottom, corresponding to $\phi_a = 0.195$, 0.254, 0.32, and 0.4. For clarity, the first three curves are shifted up by 0.915, 0.61, and 0.305, respectively, on the M axis. (c) M vs d for samples with $d_a = 0.8$ and $l_r = 175$ at varied disk density $\phi_a = 0.00212$, 0.09, 0.17, 0.254, and 0.332, from top to bottom. (d) The corresponding fraction of particles in the largest cluster C vs d for the system in panel (c).

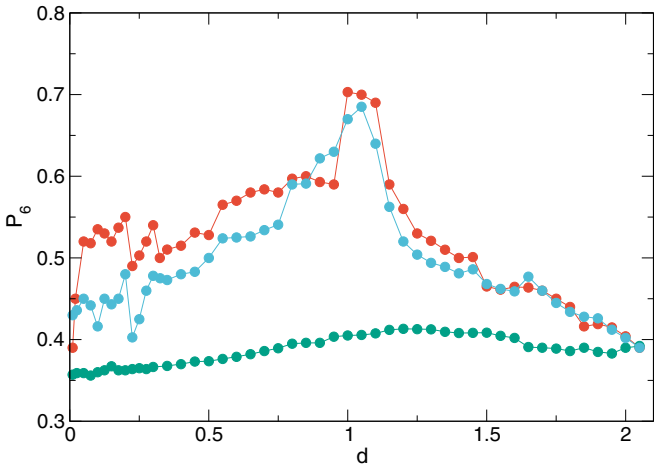

FIG. 5. The fraction of sixfold coordinated particles P_6 vs obstacle size d for the system in Fig. 1 with $d_a = 0.9$ and $l_r = 175$ at different applied drift forces of $F_D = 0.0$ (top red curve), $F_D = 0.2$ (middle blue curve), and $F_D = 1.0$ (bottom green curve).

Fig. 3(c). The onset of this locally square commensurate state shifts to lower values of d with increasing d_a. The drop in M near $d = 1.0$ in the $d_a = 0.8$ system is due to the appearance of a different type of commensurate clustering state where the ordering is triangular rather than square, similar to what is shown in Figs. 2(b) and 3(a). The triangular commensurate state persists up to $d = 1.1$ for the $d_a = 0.8$ system and appears over a slightly higher range of d in the $d_a = 0.9$ system. The peak near $d = 1.1$ for $d_a = 0.8$ is the result of the formation of a frustrated state of the type illustrated in Figs. 2(c) and 3(b). For $d_a = 1.0$, the triangular commensurate state is present near the dip in M at $d = 0.7$. In general, as d_a increases, the overall magnitude of M drops.

The behavior of M versus d for samples with $l_r = 175$ where we hold the active disk diameter fixed at $d_a = 0.8$ but consider different disk densities $\phi_a = 0.00212$, 0.09, 0.17, 0.254, and 0.332 is shown in Fig. 4(c). Since the disk radius is fixed, the locally square commensuration dip in M at $d = 1.85$ does not shift with changing ϕ_a. For $\phi_a = 0.00212$, the system is in the single-particle limit, there are no commensurate peaks or dips, and M drops to zero for $d > 2.25$ when the obstacles form a percolating barrier to motion. For $\phi_a = 0.09$ and 0.17, the triangular commensuration dip at $d = 1.0$ and the incommensuration peak at $d = 1.1$ found for larger ϕ_a are absent; however, there is a high density incommensuration peak at $d = 1.95$. When $\phi_a = 0.332$, the overall value of M decreases and an additional incommensuration peak forms at $d = 1.5$. Here, M drops to zero for $d > 1.9$ when the system enters an active clogged state.

In Fig. 4(d) we plot the largest cluster size C versus d for the system in Fig. 4(c) with varied ϕ_a. When $\phi_a = 0.00212$, C remains small, indicating the lack of any clustering in the single particle limit, while for $\phi_a = 0.09$ and $\phi_a = 0.18$, C approaches $C = 1.0$ for $d > 2.25$ and has a peak at $d = 1.8$ corresponding to the formation of local square ordering in individual substrate plaquettes. At $\phi_a = 0.254$, there are three peaks in C corresponding to the commensuration effects at $d = 1.0$, 1.35, and 1.85, as well as a dip produced by a frustrated state at $d = 1.1$. For $\phi_a = 0.332$, a clustered state appears for all values of d, which develops crystalline ordering at the three commensurate values of d.

Experimentally, the best system in which to observe the commensuration effects would be one where activity induced phase separation occurs even in the absence of obstacles. By adding periodic obstacles to such a system, the effect of the obstacle size, activity rate, and active particle density can be explored. Initial experiments could focus on the states that form in the absence of an applied drive. In Fig. 5 we plot P_6 versus d for the system in Fig. 1 with $l_r = 175$ under drift forces of $F_D = 0.0$, 0.2, and 1.0. We note that the cluster size C (not shown) is nearly featureless over this range of parameters, showing only a small systematic decrease with increasing F_D. The commensuration peak in P_6 near $d = 1.0$ is robust in the zero drive limit and in fact is even enhanced in the absence of a drive. As F_D increases, the commensuration effects begin to wash out as the clusters become broken apart by the drive. This result indicates that the commensuration effects remain robust even in the absence of a drive.

If we vary the system size for the sample in Fig. 1 but hold d and ϕ fixed, we find no change in the trends of the behavior [39]. We have focused on active particles with run-and-tumble dynamics, but we expect that our results should also apply for robots or for other types of active dynamics such as driven diffusion as long as there is motility induced phase separation. This is because the commensuration effects arise due to the locking of the spacing of the particle lattice to that of the obstacle lattice. The work by Cates and Tailleur [25] has also shown that many of the behaviors of run-and-tumble and driven diffusive systems are equivalent in general and that the primary cause of the motility-induced phase separation is the existence of a density-dependent effective particle velocity.

IV. SUMMARY

We have examined run-and-tumble active matter disks interacting with a periodic obstacle array and find active matter commensuration and frustration effects. These arise when the active matter undergoes motility-induced phase separation into a dense crystalline phase which has a natural disk spacing. When this spacing is commensurate with the lattice constant of the obstacle array, a large crystalline phase separated state can appear, whereas, for other obstacle spacings, the crystalline phase cannot fit on the substrate and we instead find a frustrated state in which the clusters are amorphous and not as large. The commensuration and incommensuration effects produce peaks and dips in the mobility, sixfold order, and cluster size as a function of changing obstacle diameter. The commensurate crystal states can have long range triangular ordering or local square ordering. At low activity or in the Brownian limit, the commensuration effects are lost.

ACKNOWLEDGMENTS

We gratefully acknowledge the support of the U.S. Department of Energy through the LANL/LDRD program for this work. This work was supported by the U.S. Department of Energy through the Los Alamos National Laboratory. Los Alamos National Laboratory is operated by Triad National Security, LLC, for the National Nuclear Security Administration of the U.S. Department of Energy (Contract No. 892333218NCA000001).

[1] P. Bak, Commensurate phases, incommensurate phases and the devil's staircase, Rep. Prog. Phys. **45**, 587 (1982).

[2] S. N. Coppersmith, D. S. Fisher, B. I. Halperin, P. A. Lee, and W. F. Brinkman, Dislocations and the commensurate-incommensurate transition in two dimensions, Phys. Rev. B **25**, 349 (1982).

[3] C. R. Woods, L. Britnell, A. Eckmann, R. S. Ma, J. C. Lu, H. M. Guo, X. Lin, G. L. Yu, Y. Cao, R. V. Gorbachev, A. V. Kretinin, J. Park, L. A. Ponomarenko, M. I. Kastnelson, Yu. N. Gornostryev, K. Watanabe, T. Taniguchi, C. Casiraghi, H.-J. Gao, A. K. Geim, and K. S. Novoselov, Commensurate-incommensurate transition in graphene on hexagonal boron nitride, Nat. Phys. **10**, 451 (2014).

[4] K. Harada, O. Kamimura, H. Kasai, T. Matsuda, A. Tonomura, and V. V. Moshchalkov, Direct observation of vortex dynamics in superconducting films with regular arrays of defects, Science **274**, 1167 (1996).

[5] C. Reichhardt, C. J. Olson, and F. Nori, Commensurate and incommensurate vortex states in superconductors with periodic pinning arrays, Phys. Rev. B **57**, 7937 (1998).

[6] G. R. Berdiyorov, M. V. Milošević, and F. M. Peeters, Novel Commensurability Effects in Superconducting Films with Antidot Arrays, Phys. Rev. Lett. **96**, 207001 (2006).

[7] S. Tung, V. Schweikhard, and E. A. Cornell, Observation of Vortex Pinning in Bose-Einstein Condensates, Phys. Rev. Lett. **97**, 240402 (2006).

[8] M. Brunner and C. Bechinger, Phase Behavior of Colloidal Molecular Crystals on Triangular Light Lattices, Phys. Rev. Lett. **88**, 248302 (2002).

[9] C. Reichhardt and C. J. O. Reichhardt, Ordering and melting in colloidal molecular crystal mixtures, Phys. Rev. E **71**, 062403 (2005).

[10] T. Brazda, A. Silva, N. Manini, A. Vanossi, R. Guerra, E. Tosatti, and C. Bechinger, Experimental Observation of the Aubry Transition in Two-Dimensional Colloidal Monolayers, Phys. Rev. X **8**, 011050 (2018).

[11] A. Ortiz-Ambriz and P. Tierno, Engineering of frustration in colloidal artificial ices realized on microfeatured grooved lattices, Nat. Commun. **7**, 10575 (2016).

[12] I. Bloch, Ultracold quantum gases in optical lattices, Nat. Phys. **1**, 23 (2005).

[13] T. Bohlein, J. Mikhael, and C. Bechinger, Observation of kinks and antikinks in colloidal monolayers driven across ordered surfaces, Nat. Mater. **11**, 126 (2012).

[14] A. Vanossi, N. Manini, and E. Tosatti, Static and dynamic friction in sliding colloidal monolayers, Proc. Natl. Acad. Sci. USA **109**, 16429 (2012).

[15] C. Reichhardt and C. J. Olson Reichhardt, Depinning and nonequilibrium dynamic phases of particle assemblies driven over random and ordered substrates: a review, Rep. Prog. Phys. **80**, 026501 (2017).

[16] D. McDermott, J. Amelang, C. J. O. Reichhardt, and C. Reichhardt, Dynamic regimes for driven colloidal particles on a periodic substrate at commensurate and incommensurate fillings, Phys. Rev. E **88**, 062301 (2013).

[17] M. Baert, V. V. Metlushko, R. Jonckheere, V. V. Moshchalkov, and Y. Bruynseraede, Composite Flux-Line Lattices Stabilized in Superconducting Films by A Regular Array of Artificial Defects, Phys. Rev. Lett. **74**, 3269 (1995).

[18] M. C. Marchetti, J. F. Joanny, S. Ramaswamy, T. B. Liverpool, J. Prost, M. Rao, and R. A. Simha, Hydrodynamics of soft active matter, Rev. Mod. Phys. **85**, 1143 (2013).

[19] C. Bechinger, R. Di Leonardo, H. Löwen, C. Reichhardt, G. Volpe, and G. Volpe, Active particles in complex and crowded environments, Rev. Mod. Phys. **88**, 045006 (2016).

[20] J. Palacci, S. Sacanna, A. P. Steinberg, D. J. Pine, and P. M. Chaikin, Living crystals of light-activated colloidal surfers, Science **339**, 936 (2013).

[21] I. Buttinoni, J. Bialké, F. Kümmel, H. Löwen, C. Bechinger, and T. Speck, Dynamical Clustering and Phase Separation in Suspensions of Self-Propelled Colloidal Particles, Phys. Rev. Lett. **110**, 238301 (2013).

[22] A. Morin, N. Desreumaux, J.-B. Caussin, and D. Bartolo, Distortion and destruction of colloidal flocks in disordered environments, Nat. Phys. **13**, 63 (2017).

[23] Y. Fily and M. C. Marchetti, Athermal Phase Separation of Self-Propelled Particles with No Alignment, Phys. Rev. Lett. **108**, 235702 (2012).

[24] G. S. Redner, M. F. Hagan, and A. Baskaran, Structure and Dynamics of a Phase-Separating Active Colloidal Fluid, Phys. Rev. Lett. **110**, 055701 (2013).

[25] M. E. Cates and J. Tailleur, Motility-induced phase separation, Annu. Rev. Condens. Matter Phys. **6**, 219 (2015).
[26] C. Reichhardt and C. J. O. Reichhardt, Active microrheology in active matter systems: Mobility, intermittency, and avalanches, Phys. Rev. E **91**, 032313 (2015).
[27] C. Reichhardt and C. J. Olson Reichhardt, Active matter transport and jamming on disordered landscapes, Phys. Rev. E **90**, 012701 (2014).
[28] A. Morin, D. Lopes Cardozo, V. Chikkadi, and D. Bartolo, Diffusion, subdiffusion, and localization of active colloids in random post lattices, Phys. Rev. E **96**, 042611 (2017).
[29] M. Zeitz, K. Wolff, and H. Stark, Active Brownian particles moving in a random Lorentz gas, Eur. Phys. J. E **40**, 23 (2017).
[30] T. Bhattacharjee and S. S. Datta, Confinement and activity regulate bacterial motion in porous media, Soft Matter **15**, 9920 (2019).
[31] O. Chepizhko and T. Franosch, Ideal circle microswimmers in crowded media, Soft Matter **15**, 452 (2019).
[32] A. Chardac, S. Shankar, M. C. Marchetti, and D. Bartolo, Emergence of dynamic vortex glasses in disordered polar active fluids, arXiv:2002.12893.
[33] G. Volpe, I. Buttinoni, D. Vogt, H.-J. Kümmerer, and C. Bechinger, Microswimmers in patterned environments, Soft Matter **7**, 8810 (2011).
[34] R. Alonso-Matilla, B. Chakrabarti, and D. Saintillan, Transport and dispersion of active particles in periodic porous media, Phys. Rev. Fluids **4**, 043101 (2019).
[35] H. E. Ribeiro, W. P. Ferreira, and F. Q. Potiguar, Trapping and sorting of active matter in a periodic background potential, Phys. Rev. E **101**, 032126 (2020).
[36] M. Brun-Cosme-Bruny, A. Förtsch, W. Zimmermann, E. Bertin, P. Peyla, and S. Rafaï, Deflection of phototactic microswimmers through obstacle arrays, Phys. Rev. Fluids **5**, 093302 (2020).
[37] S. Yazdi, J. L. Aragones, J. Coulter, and A. Alexander-Katz, Metamaterials for active colloid transport, arXiv:2002.06477.
[38] C. Reichhardt and C. J. O. Reichhardt, Directional locking effects for active matter particles coupled to a periodic substrate, Phys. Rev. E **102**, 042616 (2020).
[39] See Supplemental Material at http://link.aps.org/supplemental/10.1103/PhysRevE.103.022602 for movies illustrating the commensurate and incommensurate states and for a figure showing P_6 for different values of L.
[40] H. T. Nguyen, C. Reichhardt, and C. J. O. Reichhardt, Clogging and jamming transitions in periodic obstacle arrays, Phys. Rev. E **95**, 030902(R) (2017).